

RESEARCH ARTICLE

10.1002/2015JC011226

Key Points:

- The upper-ocean responses to TCs are analyzed in a high resolution fully coupled climate model
- High resolution coupled model is capable of simulating realistic TC-induced upper ocean responses
- Tropical cyclones can influence upper ocean mixing and heat budgets in the coupled model

Supporting Information:

- Supporting Information S1

Correspondence to:

H. Li,
huili7@illinois.edu

Citation:

Li, H., R. L. Sriver, and M. Goes (2016), Modeled sensitivity of the Northwestern Pacific upper-ocean response to tropical cyclones in a fully coupled climate model with varying ocean grid resolution, *J. Geophys. Res. Oceans*, 121, 586–601, doi:10.1002/2015JC011226.

Received 12 AUG 2015

Accepted 15 DEC 2015

Accepted article online 18 DEC 2015

Published online 21 JAN 2016

Modeled sensitivity of the Northwestern Pacific upper-ocean response to tropical cyclones in a fully coupled climate model with varying ocean grid resolution

Hui Li¹, Ryan L. Sriver¹, and Marlos Goes^{2,3}

¹Department of Atmospheric Sciences, University of Illinois at Urbana-Champaign, Urbana, Illinois, USA, ²Cooperative Institute for Marine and Atmospheric Studies, University of Miami, Miami, Florida, USA, ³NOAA/AOML, Physical Oceanography Division, Miami, Florida, USA

Abstract Tropical cyclones (TCs) actively contribute to Earth's climate, but TC-climate interactions are largely unexplored in fully coupled models. Here we analyze the upper-ocean response to TCs using a high-resolution Earth system model, in which a 0.5° atmosphere is coupled to an ocean with two different horizontal resolutions: 1° and 0.1°. Both versions of the model produce realistic TC climatologies for the Northwestern Pacific region, as well as the transient surface ocean response. We examined the potential sensitivity of the coupled modeled responses to ocean grid resolution by analyzing TC-induced sea surface cooling, latent heat exchange, and basin-scale ocean heat convergence. We find that sea surface cooling and basin-scale aggregated ocean heat convergence are relatively insensitive to the horizontal ocean grid resolutions considered here, but we find key differences in the poststorm restratification processes related to mesoscale ocean eddies. We estimate the annual basin-scale TC-induced latent heat fluxes are $1.70 \pm 0.16 \times 10^{21}$ J and $1.43 \pm 0.16 \times 10^{21}$ J for the high-resolution and low-resolution model configurations, respectively, which account for roughly 45% of the total TC-induced ocean heat loss from the upper ocean. Results suggest that coupled modeling approaches capable of capturing ocean-atmosphere feedbacks are important for developing a complete understanding of the relationship between TCs and climate.

1. Introduction

Increasing evidence suggests TCs play an active role in influencing the dynamics of the coupled ocean-atmosphere system [Emanuel, 2001; Hart, 2011; Sriver et al., 2008, 2010; Sriver and Huber, 2007]. Several recent studies have shown that enhanced upper-ocean mixing, associated with extreme TC winds, could lead to positive ocean heat convergence (OHC) [Buetti et al., 2014; Emanuel, 2001; Jansen et al., 2010; Mei et al., 2013; Mei and Pasquero, 2012; Park et al., 2011; Sriver, 2013; Sriver et al., 2010; Sriver and Huber, 2007], which may potentially alter large-scale circulations and transports of the ocean-atmosphere system [Boos et al., 2004; Emanuel, 2001; Hu and Meehl, 2009; Jansen and Ferrari, 2009; Pasquero and Emanuel, 2008; Sriver and Huber, 2010]. These TC processes and feedbacks are generally not captured in current numerical models used for climate projections, but their representation may be necessary to reduce uncertainty in projections of climate change impacts.

Numerical models are useful tools to explore the relationship between TCs and climate. Many uncoupled atmosphere and ocean modeling experiments have pointed to important climate connections associated with TCs. High-resolution atmosphere models have demonstrated skill in simulating realistic TC-like circulations and basin-scale climatologies, and they have been used to examine the sensitivity of TC activity to prescribed changes in climate [Bacmeister et al., 2013; Camargo et al., 2005; Wehner et al., 2010], and increasing atmosphere model grid resolution can significantly improve the representation of simulated TCs [Bacmeister et al., 2013; Li et al., 2013; Manganello et al., 2012; Murakami and Sugi, 2010; Strachan et al., 2012; Walsh et al., 2013; Wehner et al., 2014]. In addition to atmosphere-only experiments, ocean-only models have been used extensively to analyze the oceanic response to TC forcing, including TC influences on ocean heat convergence [Jansen and Ferrari, 2009; Vincent et al., 2013], mixing budgets [Huang et al., 2009; Mei and Pasquero, 2012], and large-scale ocean heat transport and circulations [Buetti et al., 2014; Jansen and Ferrari, 2009; Jullien et al., 2012; Sriver et al., 2010; Sriver and Huber, 2010; Vincent et al., 2013; Wang et al., 2014].

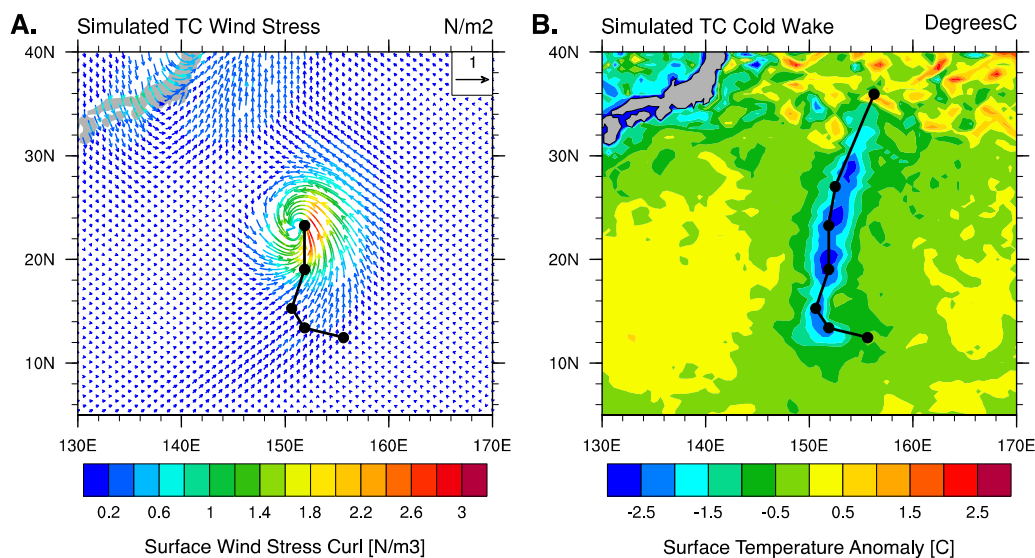


Figure 1. (a) Simulated TC circulation using CCSM3.5 with a 0.5° atmosphere model. (b) The corresponding surface temperature anomaly from the 0.1° eddy-resolving ocean component. The temperature anomaly is estimated as the poststorm minus prestorm temperature fields.

Ocean-atmosphere coupling is important for quantifying surface fluxes of heat and momentum within storm-affected regions [Bender and Ginis, 2000; Jullien *et al.*, 2014], as well as potential remote impacts associated with altered dynamics [Bender and Ginis, 2000; Jullien *et al.*, 2014; Pasquero and Emanuel, 2008; Scoccimarro *et al.*, 2011]. Several recent modeling studies have shown that coupled climate models are capable of simulating present-day TC statistics, including geographical distribution, frequency, and interannual variability [Bell *et al.*, 2013; Gualdi *et al.*, 2008; Kim *et al.*, 2014; Rathmann *et al.*, 2014]. These models typically exhibit biases across different basins due to their generally coarse model resolution, relatively short simulation times, and/or uncertainties related to integrated model responses and interactions. Coupled climate models have also been used to explore potential TC connections to large-scale climate features. For example, Hu and Meehl [2009] use a relatively coarse resolution ($\sim 2.8^\circ$ atmosphere $\sim 1^\circ$ ocean) version of the Community Climate System Model (CCSM), to explore the effect of TCs on meridional volume and heat transports, finding that the positive influence of TC-induced diapycnal ocean mixing on meridional transports is partially modulated by increased freshwater forcing associated with heavy TC precipitation. Also using a relatively low-resolution version of CCSM3, Manucharyan *et al.* [2011] analyzed how imposed intermittent vertical ocean mixing associated with TC events may affect large-scale ocean temperature structure and circulation patterns. They found that the additional TC-like mixing leads to both enhanced poleward ocean heat transport and tropical equatorial heat convergence. Scoccimarro *et al.* [2011] investigated the North Hemisphere poleward ocean heat transport induced by model-generated TCs on both transient and long-term time scales with a 0.75° atmosphere and 2° ocean. They concluded that TCs could largely enhance the ocean heat transport on weekly time scales, but the effect is negligible when considering annually averaged ocean heat transport.

These past studies have provided fundamental insights into the potential relationship between TCs and climate, but they are generally limited by relatively coarse ocean grid resolution and a lack of appropriate ocean-atmosphere coupling for analyzing TC effects in the coupled system. While several studies [e.g., Wehner *et al.*, 2014] have investigated the effects of increased atmosphere resolution on TC climatologies, the sensitivity of the upper-ocean response to ocean grid resolution has not been adequately addressed within coupled model frameworks. Here we analyze the upper-ocean response to TCs using a high-resolution configuration of the Community Climate System Model version 3.5 (CCSM 3.5) [Kirtman *et al.*, 2012], which features an atmosphere model with 0.5° horizontal resolution coupled to an ocean model with two different horizontal resolutions (1° and 0.1°). This model is capable of simulating realistic TC circulations and cold wakes (Figure 1), as well as TC-induced subsurface thermocline warming [McClellan *et al.*, 2011]. We use the results of the model experiments to analyze TC climatologies, the transient upper-ocean response

to TC passage, and basin-scale aggregated TC effects on ocean heat convergence and surface heat fluxes. We focus our analysis on the Northwestern Pacific Ocean, which represents a region exhibiting a realistic TC climatology and seasonal variability within both model configurations. A key goal of this paper is to examine the potential sensitivity of the coupled modeled response to increasing ocean grid resolution toward scales capable of resolving mesoscale ocean eddies.

This paper is organized as follows. Section 2 describes the model, observational data, TC tracking scheme, and methods for the OHC calculations. Section 3 is the main results section, which is divided into three parts. We first analyze and compare the modeled TC climatologies of the two model configurations. We then investigate the sensitivity of surface responses, including surface cooling and latent heat fluxes, to ocean grid resolution. In particular, the sensitivities are further examined by analyzing potential effects of parameterized versus resolved mesoscale ocean eddies. Lastly, we show first-order estimates of the basin-scale annual mean TC-induced latent heat budget and ocean heat convergence within the coupled model. The caveats of this study are discussed in section 4. The main conclusions and implications of this work are summarized in section 5.

2. Data and Methods

2.1. Model Description

We analyze model output from a set of century-scale present-day control simulations using high-resolution configurations of CCSM 3.5 [Gent *et al.*, 2010; Kirtman *et al.*, 2012; McClean *et al.*, 2011]. CCSM3.5 is a pre-release version of CCSM4 and includes the Community Atmospheric Model (CAM) version 3.5 [Gent *et al.*, 2010] coupled to the Parallel Ocean Program (POP) version 2 [Danabasoglu *et al.*, 2012; Gent *et al.*, 2010]. The modeling experiment consists of two simulations in which the 0.5° atmosphere component model is coupled to two different versions of the ocean model. The low-resolution control simulation features ocean and sea-ice components with a nominal 1° horizontal resolution, with constant grid spacing in the zonal direction (1.2°) and varying grid spacing in the meridional direction (0.27° at the equator to 0.54° in the mid-latitudes). The high-resolution control simulation features ocean and sea-ice components with a uniform 0.1° horizontal spacing at the equator, and reducing to $\sim 0.02^\circ$ at high latitudes. Both ocean model versions have 42 vertical levels with thickness varying from 10 m at the surface to 250 m at 6000 m depth. Momentum and heat fluxes at the air-sea interface are computed by the coupler and are shared among model components. Surface wind stress is calculated using relative wind, which refers to the difference between lowest model level wind and ocean current velocities. Ocean vertical mixing is parameterized using K-profile parameterization (KPP) scheme. Kirtman *et al.* [2012] find that small-scale features resolved in the high-resolution ocean model (e.g., mesoscale eddies) can alter large-scale climate conditions, such as global mean temperature, general circulation patterns, Arctic sea ice losses, rainfall, ocean stratification, climate variability, and air-sea interactions.

The simulations include over 100 years of monthly output from the ocean and atmosphere models, of which roughly 20 years of output also include a subset of daily surface variables. We focus our analysis primarily on the 20 years of daily surface output for analyzing the transient TC effects. Available daily variables from the model simulations include surface wind stress, surface temperature, surface latent and sensible heat fluxes, and precipitation rate. The daily model output does not contain any subsurface ocean variables. Our analysis is limited by the lack of daily subsurface ocean information; however, the available atmosphere surface outputs enable us to perform comprehensive sensitivity analyses of the transient TC-induced responses near the ocean-atmosphere interface. In addition, we analyze basin-scale TC-induced ocean heat budgets using previously published methods that combine daily surface temperature information with monthly vertical temperature profiles [Srifer *et al.*, 2008] (see section 2.4), which are available for these simulations. These methods have been shown to provide robust first-order estimates of transient ocean heat uptake compared to altimetry-based estimates [Mei *et al.*, 2013]. Note that such methods may overestimate the ocean heat uptake considering the importance of the variations in the prestorm stratification [Vincent *et al.*, 2012b], vertical advection [Jullien *et al.*, 2012], and thermocline seasonal variations [Jansen *et al.*, 2010]. These limiting assumptions provide important constraints on the first-order estimates of surface fluxes and ocean heat convergence.

2.2. Tropical Cyclone Detection and Tracking Algorithm

We developed an algorithm to identify TC-like circulations in the model. The algorithm is adapted from previous studies analyzing TCs in atmosphere-only simulations [Camargo and Zebiak, 2002; Zhao et al., 2009], based on the availability of daily variables outlined in section 2.1. We identify a TC-like circulation within the model using the following criteria: (1) cyclogenesis occurs within 30° of the equator; (2) the maximum surface wind stress curl exceeds $2 \times 10^{-6} \text{ N m}^{-3}$, and maximum 10 m wind speed exceeds 15 m s^{-1} corresponding to a relaxed threshold for the minimum wind speed for a tropical storm; (3) the horizontal scale is larger than 200 km; (4) the storm center must not be stationary for more than 24 h; and (5) the event must last for at least 3 days. Criteria (3) and (4) are important constraints to filter standing ocean eddies, since we are using relative wind (differences between 10 m wind and ocean current) derived from surface wind stress as the basis for constructing TC surface wind fields. Several of our criteria are consistent with previous TC detection methods [Camargo and Zebiak, 2002; Zhao et al., 2009], however, some differences are necessary given the limited number of variables available from the model output. For example, maximum surface wind stress curl is used to identify and locate a potential TC storm center, rather than the 850 hPa vorticity and minimum sea level pressure. In addition, the cyclone core structure is not considered here. We have performed multiple sensitivity tests to optimize the detection and tracking algorithms and we calibrate the threshold values for each variable. Results are visually inspected to ensure the characteristics of the identified circulations are consistent with TC events (Figure 1). Additional details about the procedure can be found in supporting information.

2.3. Observational Data

We use the Optimally Interpolated Sea Surface Temperature (OI SST) data product to analyze observed TC-induced near-surface ocean temperature responses. The OI SST is a hybrid product of the Tropical Rainfall Measuring Mission's (TRMM) Microwave Imager (TMI) and the Advanced Microwave Scanning Radiometer (AMSRE) data, which provides complete daily SST at 0.25° horizontal resolution from 2002 to present [Gentemann et al., 2010]. We analyze all TCs globally between 2003 and 2012 as defined by the best track data set, which combines track information from NOAA's Storm Prediction Center and the U.S. Navy's Joint Typhoon Warning Center. The best track product categorizes TC tracks within five different regions: North Atlantic, East Pacific, West Pacific, Indian Ocean, and Southern Hemisphere. We analyze subsurface ocean properties using potential temperature profiles and mixed-layer depths from the European Center for Medium-Range Weather Forecast Ocean Reanalysis System 4 (ECMRWF ORAS4), providing monthly ocean state information between 1957 and present. Climatological mixed-layer depth and SST in ORAS4 are compared with that from the World Ocean Atlas 2013 (WOA13) [Locarnini et al., 2013] to ensure validity of this data set (supporting information Figures S5–S8). Annually and seasonally averaged observational wind data are from National Center for Climate Prediction/National Center for Atmospheric Research (NCEP/NCAR) reanalysis. Monthly averaged eddy kinetic energy (EKE) is derived from 17 years (1993–2010) of monthly averaged sea surface height anomalies (SSA) [Le Traon et al., 1998], produced by Ssalto/Duacs and distributed by Aviso. The data are a gridded $1/4^\circ \times 1/4^\circ$ global product merged from several altimeter satellite missions. The sea level anomalies are referenced to a 20 year period (1993–2012).

2.4. Calculation of TC-Induced Ocean Heat Convergence (OHC)

The TC-induced, vertically integrated OHC is estimated following previous methods [Emanuel, 2001; Srivier et al., 2008; Srivier and Huber, 2007]:

$$OHC = \iiint F \Delta T dh dW dL, \quad (1)$$

where F is the fraction of heat transported downward through the base of the oceanic mixed layer through mixing and entrainment, ΔT is the magnitude of surface temperature anomaly, dh is the depth of vertical mixing, and dW and dL are the cross-track and along-track length of the storm wake. Seawater density ρ and heat capacity C are held constant at 1020 kg/m^3 and $3900 \text{ J/(kg } ^\circ\text{C)}$, respectively. In order to estimate F , we analyze surface latent heat exchange during TC days, as it is the second largest contributor to sea surface cooling [Huang et al., 2009] (see section 3.3). We employ a footprint method that samples surface properties within a $6^\circ \times 6^\circ$ domain (dW and dL), which is centered on the best track location and moves with the storm. The footprint domain size is consistent with area sizes used in other studies [Cheng et al., 2014; Lloyd and Vecchi, 2011; Mei and Pasquero, 2012; Srivier and Huber, 2007]. At each storm location, temperature

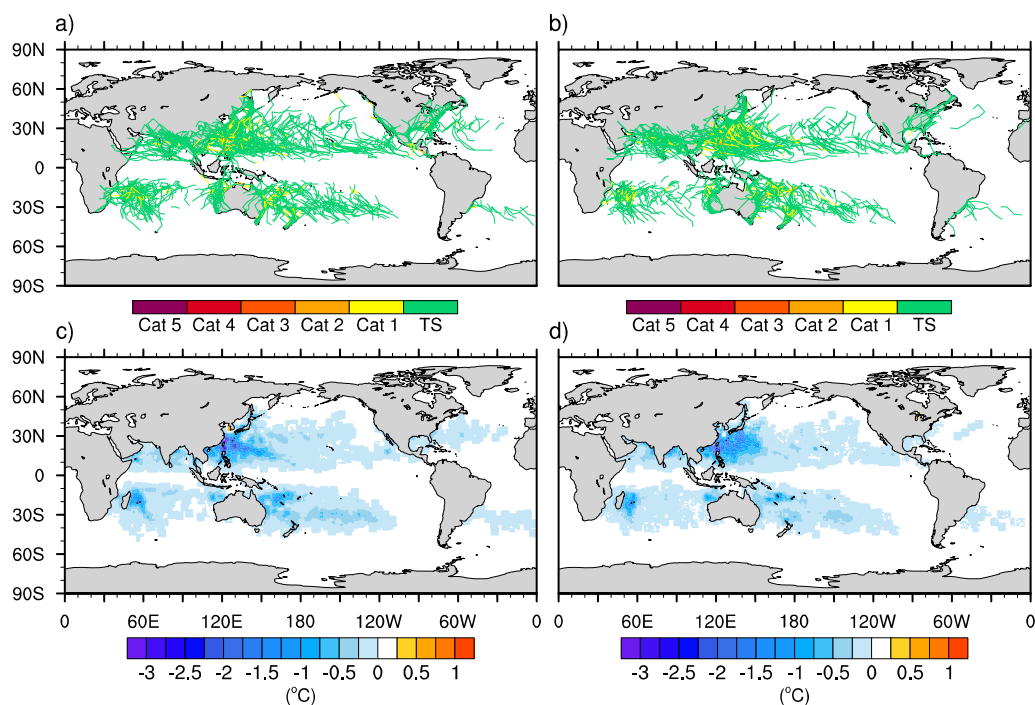


Figure 2. Model-simulated storm tracks accumulated over 20 years in the (a) low-resolution and (b) high-resolution configurations. Modeled annually accumulated, storm-induced average sea surface cooling for the (c) low-resolution and (d) high-resolution configurations.

anomalies are calculated using SST from 2 days after storm passage relative to the average SST between 12 and 5 days prior to the storm. Sensitivity analyses were performed to choose characteristic sizes of the footprint domain and time interval, and we chose values that maximized the TC effect. The results presented here are generally insensitive to the choice of spatial and temporal sampling scales, particularly for the comparison between model simulations with varying ocean grid resolution.

We use three different strategies for estimating TC-induced mixing depths that we apply to both model simulations and observations. First, we assume a uniform and constant mixing depth of 50 m, consistent with past case study analysis [D'Asaro *et al.*, 2007] and methods used in previous observation-based studies [Srifer and Huber, 2007]. For the second method, we assume that vertical mixing for all storms penetrates to levels corresponding to the monthly climatological mixed-layer depth at each grid point. In the third method, we combine the TC-induced SST anomalies with monthly climatological vertical ocean temperature profiles to estimate mixing depth as the level from which water must be upwelled to achieve the observed surface temperature anomaly [Srifer *et al.*, 2008]. In this method, mixing depth is calculated as $dh = \Delta T \cdot \partial z / \partial T$, where ΔT is the TC-induced SST anomaly and $\partial z / \partial T$ is the inverse of the vertical temperature gradient obtained from the monthly climatological ocean temperature at each location. All three methods likely underestimate the actual TC-induced vertical mixing length scale, but we chose these criteria in order to examine the robustness of the model's response and resolution dependence under uncertain assumptions. Ocean heat convergence on each grid point is then calculated individually before being integrated across the footprint domain, to account for any nonuniform cooling anomalies within the domain.

3. Model Results and Discussion

3.1. Modeled Tropical Cyclone Number and Climatology

TC tracks accumulated over 20 years in both versions of the model are shown in Figures 2a and 2b. We find that both the low-resolution and high-resolution simulations generally capture the spatial distribution of the global storm tracks. However, both model configurations exhibit several key limitations. The total number of storms globally is roughly 50% of the observed current-day climatology (Table 1). The annual TC counts in the north Atlantic and east Pacific basins are too low compared to observed climatologies (Figure 3). For the

Table 1. Modeled and Observation-Based Annual Storm Number

Number	OBS	LRC	HRC
Annual global storm number	92	45.7	45.3
Annual storm number in Northwestern Pacific	26.5	15.4	16.6

environmental factors for TC development. The model also simulates storms in the South Atlantic basin, which are rarely observed in nature. The cause may be due to anomalously low vertical wind shear and warm SST in this region compared to observations (supporting information Figures S1 and S2).

In addition, the model does not capture storm intensities greater than Category 3 (Figure 2). The storm intensity distributions are similar between the two versions of the model, and they are shifted toward low values compared to observations (Figure 4). The biases in intensity and number are likely linked to the relatively coarse

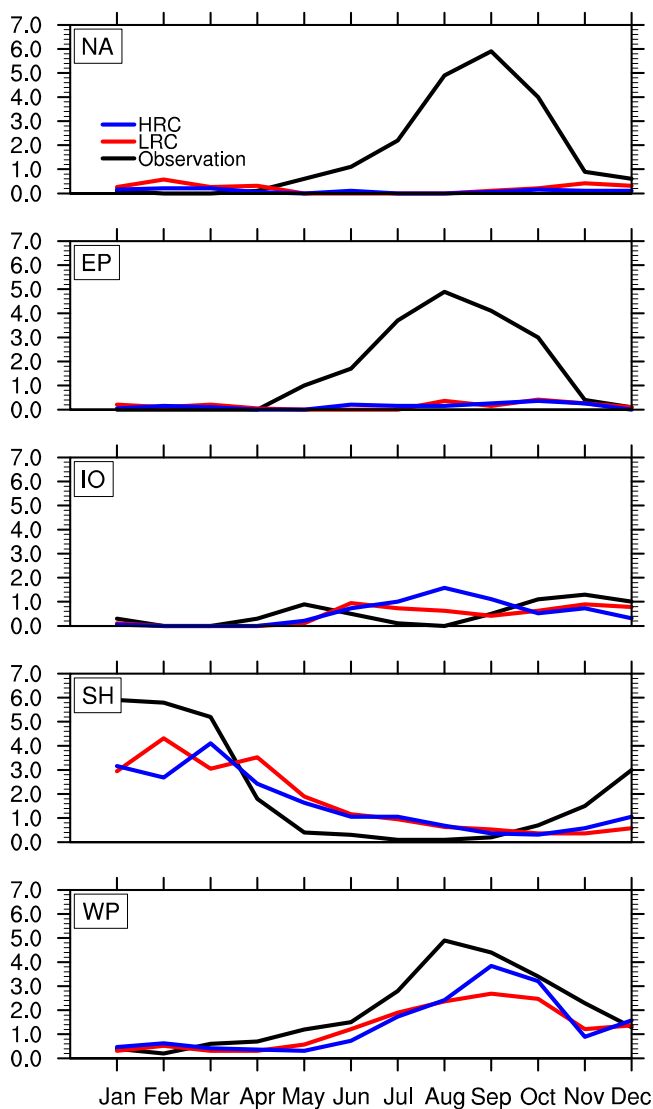


Figure 3. Monthly averaged storm counts in five tropical cyclone basins: (top to bottom) North Atlantic, East Pacific, Indian Ocean, South Hemisphere, and Northwest Pacific. Red and blue curves represent results from the low and high-resolution model simulations, respectively. Black curves indicate observation-based results only considering TC up to Category 3 to enable direct comparison with model results.

north Atlantic region, the bias may be attributed to relatively low annual SST (supporting information Figure S1) and relatively high vertical wind shear (supporting information Figure S2) within the Main Development Region for both simulations, which are both important envi-

ronmental factors for TC development. The model also simulates storms in the South Atlantic basin, which are rarely observed in nature. The cause may be due to anomalously low vertical wind shear and warm SST in this region compared to observations (supporting information Figures S1 and S2). In addition, the model does not capture storm intensities greater than Category 3 (Figure 2). The storm intensity distributions are similar between the two versions of the model, and they are shifted toward low values compared to observations (Figure 4). The biases in intensity and number are likely linked to the relatively coarse (0.5°) atmosphere component resolution [Li et al., 2013; Shaevitz et al., 2014; Strachan et al., 2012; Zhao et al., 2009], and similar limitations are common among other Earth system models [Camargo, 2013]. Recent findings using newer versions of CAM with higher horizontal grid resolution (0.25°) show significant improvements in the total number, although biases still exist in the storm intensity and spatial distribution [Bacmeister et al., 2013; Wehner et al., 2014]. The intensity bias may also be due to the different methods of computing daily-averaged storm wind speed between observations and model output. The best track daily wind product represents the average of the 6 h instantaneous maximum winds. The daily wind from the model is averaged over the entire day given the daily ocean model output frequency, which would smooth out the peak wind speed and lead to a low-bias compared to averages of 6 h instantaneous winds. To test the hypothesis that the wind bias is due to the differences in time-averaging, we analyzed 5 years of storm intensity distributions using a separate high-resolution (0.25° atmosphere, 0.1° ocean) CESM-coupled simulation [Small et al., 2014] where daily and 6 h output frequencies are both available for the same time period. We found that while the intensity distribution from the 6 h output is quite consistent with observations, the distribution computed from the daily output exhibits a similar low bias to our current model analysis (supporting information Figure S3). This suggests that climate models with 6 h output frequency

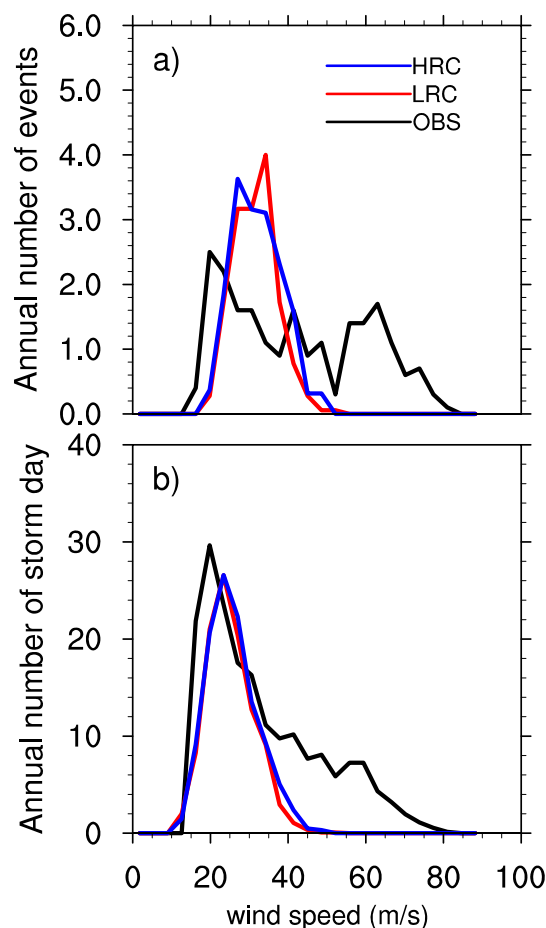


Figure 4. Frequency distributions of (a) the maximum wind speed of each tropical cyclone event and (b) the wind speed of each storm day in the Northwestern Pacific basin for observations (OBS), low-resolution configuration (LRC), and high-resolution configuration (HRC). Here we only consider storm days with wind speed exceeding 15 m s^{-1} .

accumulated TC-induced surface cooling in the model is generally lower compared to observations, which is due primarily to the model's underrepresentation of the TC number and intensity. In addition, the modeled surface temperature response is generally insensitive to horizontal ocean grid resolution, and the biases are minimal in the Northwestern Pacific region.

In order to diagnose the transient response of upper-ocean temperature to TC passage, we analyze time series composites of the area-averaged SST anomalies for the low-resolution and high-resolution simulations (Figure 5). The anomalies are referenced to the prestorm conditions (Figure 5, right), which are defined as the average SST over 12–5 days before the storm arrival, as well as to the 20 year daily climatology (Figure 5, left). Comparing against climatologies can be useful to remove seasonal effects on time scales longer than a few weeks. We test the sensitivity of the SST response to the averaging domain size using multiple footprints ($2^\circ \times 2^\circ$, $6^\circ \times 6^\circ$, $10^\circ \times 10^\circ$). In both model simulations, SST begins to decrease 2–3 days prior to the storm arrival, and it reaches a minimum 2 days following passage of the storm center. The magnitude of the maximum cooling is generally consistent between the two configurations. However, the high-resolution configuration shows cooling approximately 0.1°C stronger than the low-resolution configuration within the $2^\circ \times 2^\circ$ averaging footprint size, which may be due to differences in horizontal advection or surface heat fluxes (discussed in section 3.2.2). This difference is smoothed out when averaged over a larger area. In both versions of the model, the time scales of SST restoration to climatologically normal conditions are much longer than suggested by the observations [Dare and McBride, 2011; Lloyd and Vecchi, 2011; Mei and Pasquero, 2012]. In the high-resolution configuration, SST returns to climatology about 120 days

exhibit more accurate TC intensity distributions when comparing model output with best track data. Despite these biases, we find the CCSM3.5 model captures the observed seasonal variability in several key basins (see Figure 3), including the Northwestern Pacific region, which is where we focus our analysis.

The consistency in storm intensity distribution suggests that both versions of the model represent similar climatological environmental conditions important for TC intensity. The effect of prestorm SST is of particular interest here, since it may be sensitive to the representation of meso-scale eddies. In order to diagnose the sensitivity of prestorm SST to model resolution, we analyzed the frequency distribution of SST anomalies 3 days prior to storm passage for all storm days (supporting information Figure S4). The anomalies are referenced to daily climatological values. The results show no significant difference in the distributions, suggesting that eddies do not have a major impact on prestorm SST conditions in the model.

3.2. Modeled TC-Induced Sea Surface Responses

3.2.1. Spatial and Temporal Characteristics of Sea Surface Cooling

The annual averages of the accumulated TC-induced temperature anomalies for each version of the model are shown in Figures 2c and 2d. Both model versions exhibit spatial patterns of cooling that are consistent with previous observation-based analyses [Srifer *et al.*, 2008; Srifer and Huber, 2007]. The magnitude of the

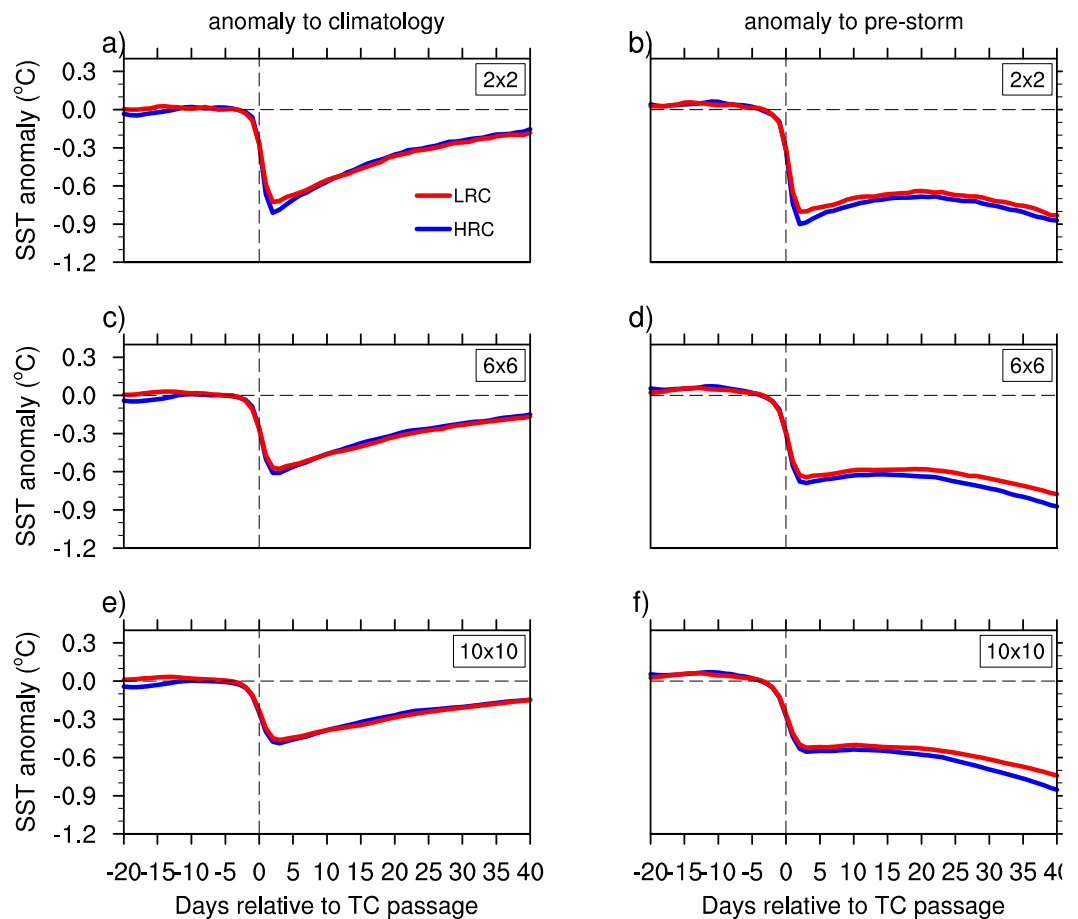


Figure 5. Temporal evolution of composite TC-induced sea surface temperature anomalies relative to (a, c, e) daily climatology and anomalies relative to (b, d, f) prestorm conditions in the Northwest Pacific basin for low-resolution simulation (LRC) and high-resolution simulation (HRC). The SST anomaly is averaged over a (top) $2^\circ \times 2^\circ$, (middle) $6^\circ \times 6^\circ$, and (bottom) $10^\circ \times 10^\circ$ TC footprint domain that moves with the storms.

later; in the low-resolution configuration, the cold anomaly persists even after 200 days, which is similar to recent results of an ocean-only modeling experiment [Jullien *et al.*, 2012].

3.2.2. Temporal Evolution of Surface Latent Heat Exchanges

The temporal evolution of the surface latent heat fluxes during storm passage is shown in Figure 6. Similar to the analyses of the surface cooling, we averaged the latent heat fluxes using different footprint sizes centered on the TC center. Latent heat fluxes are represented as total values (Figure 6, right), as well as anomalies referenced to the long-term mean daily climatology (Figure 6, left). In both versions of the model, latent heat fluxes begin to increase about a week before the storm's arrival, indicating an anomalous heat supply from the ocean to the atmosphere prior to the storm. The coupled model shows a spike on the day of the storm passage, and the peak value of the daily heat fluxes in the high-resolution version is slightly higher than its low-resolution counterpart across all the footprint sizes.

Using the $6^\circ \times 6^\circ$ footprint domain, we find the long-term mean climatological daily average latent heat fluxes without TC forcing is 158 W m^{-2} (145 W m^{-2}) in the high (low)-resolution ocean configuration, while the latent heat flux under TC conditions is 270.61 W m^{-2} (241.75 W m^{-2}) in the high (low)-resolution configuration. The magnitudes of latent heat fluxes with and without TCs are both consistent with the observational estimates based on Hurricane Isabel using high-resolution satellite-derived dataset [Liu *et al.*, 2011]. We use an observation-based case study of the Category 4 hurricane Frances in 2004 [Huang *et al.*, 2009], as a first-order constraint on the modeled fluxes. Huang *et al.* [2009] estimate the daily-averaged latent heat fluxes aggregated over a 400 km area on the day of the maximum intensity is 0.09 PW. In the current study, the two strongest daily-averaged storm winds are 50 m s^{-1} in low-resolution version and 50.3 m s^{-1} in

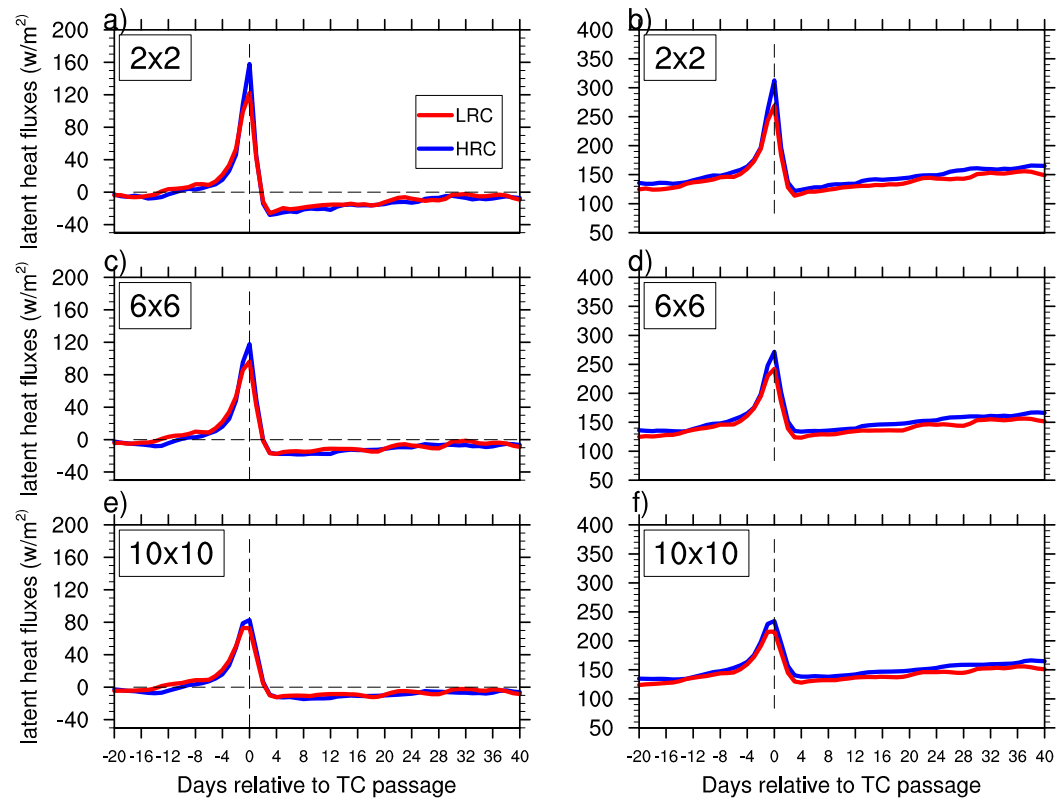


Figure 6. Temporal evolution of composite TC-induced surface latent heat fluxes anomalies relative to (a, c, e) daily climatology and their (b, d, f) total values in the Northwest Pacific basin for low-resolution simulation (LRC) and high-resolution simulation (HRC). The latent heat flux anomaly is averaged over a (top) $2^\circ \times 2^\circ$, (middle) $6^\circ \times 6^\circ$, and (bottom) $10^\circ \times 10^\circ$ footprint domain that moves with the storms.

high-resolution version. Since the daily-averaged wind would underestimate the storm intensity (for reasons discussed in section 3.1), it is possible that instantaneous winds may reach Category 4 (sustained wind $>58 \text{ m s}^{-1}$). The corresponding latent heat flux peak values integrated over a 400 km area are 0.12 and 0.14 PW, which are on the same order with the estimate of *Huang et al.* [2009].

The model also captures the reduction of latent heat fluxes caused by the cold wake after TC passage. The fluxes decrease by $\sim 30 \text{ W m}^{-2}$ when averaged over the 2° area and $\sim 20 \text{ W m}^{-2}$ when averaged over the 6° area, representing $\sim 13\text{--}20\%$ decrease compared to the prestorm values. The reduction in latent heat fluxes is consistent with observation-based studies [*D'Asaro et al.*, 2007; *Liu et al.*, 2011], indicating that the coupled model approaches with a dynamic ocean may be capable of realistically capturing the negative feedbacks on TC intensification missing from atmosphere-only simulations.

3.2.3. Potential Modeled Effects of Mesoscale Ocean Eddies on TC Wake Recovery

Horizontal ocean grid resolution may be important for simulating the storm-scale transient dynamic responses. In particular, the upper-ocean restratification following TC wakes may be influenced by mesoscale eddy transport and mixing [*Haney et al.*, 2012]. Mesoscale eddies' horizontal scales are of the order of the baroclinic Rossby radius of deformation, typically of $O(10 \text{ km})$ [e.g., *Killworth*, 1997; *Chelton et al.*, 1998]. These effects are largely parameterized in the 1° version of the model and explicitly resolved in the 0.1° model.

To explore the effect of mesoscale eddies on the TC-induced upper-ocean response, we analyzed TC activity within regions of high and low annual mean eddy kinetic energy (EKE) for both models and satellite-based observations [*Le Traon et al.*, 1998]. We estimate EKE using monthly sea surface height anomalies (SSHA) in both the observational data and model output. The global annual mean EKE for the model simulations and observations are shown in Figure 7. Both versions of the model generally capture the spatial distribution of EKE, but the 0.1° model exhibits substantial improvement in the magnitude of EKE compared to the 1° ocean model [see also *Maltrud and McClean*, 2005; *Smith et al.*, 2000].

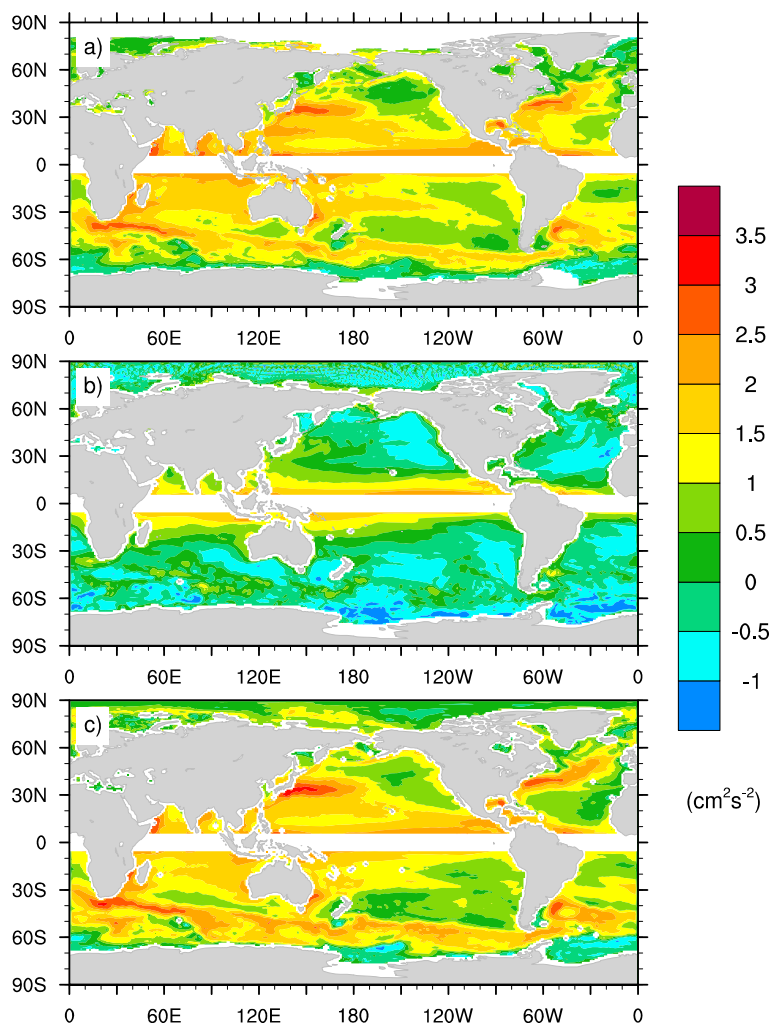


Figure 7. Logarithm of the annually averaged eddy kinetic energy (EKE) of (a) satellite-based observations, (b) low-resolution model simulation, and (c) high-resolution model simulation.

We first examine the potential relationship between wake recovery and background EKE by analyzing average wake responses within a high EKE region (30°N – 40°N , 130° – 175°), corresponding to large eddy activity within the Kuroshio current and extension. We analyzed the time series composites of the area-averaged ($2^{\circ} \times 2^{\circ}$) SST anomalies and their e -folding recovery time scales, which is defined as the number of days necessary for the SST anomaly to return to e^{-1} of the maximum cooling (Figure 8). The two model versions exhibit similar characteristics, including the fluctuating pattern of SST time series, the magnitudes of maximum cooling, and the e -folding time scales of 13 days.

We performed further analyses regarding the relationship between EKE, SST cooling and e -folding time by including all the storm days globally, in an attempt to gain additional insight into the sensitivity of the responses to ocean grid resolution. Figure 9 shows the relationship between EKE and e -folding time (upper), and between EKE and maximum SST cooling (lower). EKE is normalized in the right figures, in which the circles are bin averages and the error bars are their respective standard errors. Results indicate that although the EKE magnitudes are very different between the model simulations and observations, the TC-induced responses exhibit similar patterns when using normalized EKE. In particular, the e -folding time in the high EKE regions are generally consistent between observations and the 0.1° ocean simulation, suggesting the potential importance of eddies in wake recovery and possible improvement of the 0.1° ocean model over the 1° model. However, the relevance and robustness of this result is difficult to interpret given the disparity in the magnitude of EKE between model simulations and lack of subsurface ocean information from the model output.

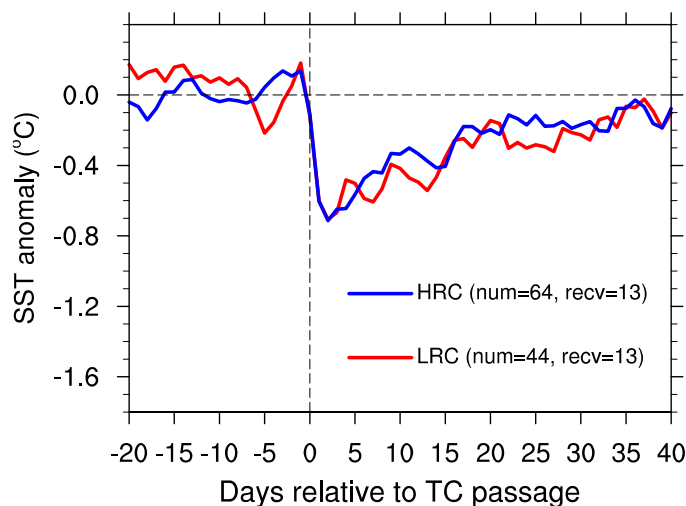


Figure 8. Temporal evolution of composite TC-induced sea surface temperature anomaly relative to daily climatology in the high EKE region (30°N–40°N, 130°–175°) for high-resolution configuration (HRC) and low-resolution configuration (LRC). The number of storm days and the average e -folding time scales are denoted in the parentheses.

3.3. First-Order Estimates of TC-Induced Upper-Ocean Energy Budget

Despite the lack of subsurface ocean fields, the availability of daily surface properties and monthly subsurface ocean temperature enables us to estimate the modeled basin-scale TC-induced OHC using different strategies accounting for mixing depth (discussed in section 2.4). The results are summarized in Figure 10. The average TC mixing depths and their corresponding OHC estimates are sensitive to the choice of vertical mixing length-scale calculation; however, the modeled OHC estimates are generally consistent between the two simulations for each mixing depth calculation. Differences between the two simulations may be partly

attributed to variations in the background ocean state (supporting information Figure S4), since the upper-ocean temperature structure in the high-resolution model exhibits stronger stratification effects than the low-resolution model. We find that varying mixing depths based on the climatological vertical ocean temperature gradients leads to the largest estimation of TC-induced OHC. This is because the location of the most significant surface cooling corresponds to areas with the deepest mixing, as indicated by the large spread over the mean mixing depth for this method (Figure 10a). In contrast, defining the mixing length based on the depth of the climatological mixed layer yields the smallest TC-induced OHC. This method likely underestimates the effect of TCs on the vertical redistribution of ocean heat, even for relatively low intensity storms considered here, because TC-induced mixing typically penetrates to depths significantly below the base of the seasonal mixed layer.

In addition to vertical mixing, TC-induced latent heat fluxes can also contribute to ocean surface cooling. Coupled modeling frameworks have the advantage of capturing surface fluxes within TC regions. We have shown in section 3.2.2 that both versions of the model are capable of simulating surface latent heat responses to TCs that are generally consistent with observations. Here we estimate the basin-scale annually accumulated TC-induced latent heat budget within the coupled model and its contribution to the total upper-ocean heat loss during TC passage.

For each storm day, we integrate the daily average latent heat fluxes from day 0 to day 2 relative to TC passage over a 6° domain. The period of 0–2 days is chosen in order to account for all the latent heat exchange responsible for the total upper-ocean heat loss, which we estimate with the maximum SST cooling that occurs on day 2 (see Figure 5). The annually accumulated basin-scale latent heat fluxes are $1.70 \pm 0.16 \times 10^{21}$ J in the high-resolution model and $1.43 \pm 0.13 \times 10^{21}$ J in the low-resolution model, representing 47 and 45% of the total TC-induced OHC estimates in the high and low-resolution model configurations, respectively (see also Table 2). This contribution of latent heat exchange is similar to the estimate of Vincent *et al.* [2012a], who found ~43% of ocean heat anomalies are due to latent heat fluxes. Results suggest that surface latent heat fluxes account for a substantial amount of heat loss from the upper-ocean during TC events, which may have important implications for global heat and energy budgets in coupled models.

We apply the basin-scale latent heat flux as a constraint on the oceanic heat convergence induced by TCs in the model simulations (corresponding to $F = 0.53$ (0.55) in the high (low)-resolution version in equation (1)). Using the varying mixing depth strategy, we estimate the modeled TC-induced, surface flux-corrected annual Northwestern Pacific basin-scale OHC to be 0.17×10^{22} J in the low-resolution simulation and 0.19×10^{22} J in the high-resolution simulation, corresponding to a mean annual rate of 0.05 ± 0.005 PW (1

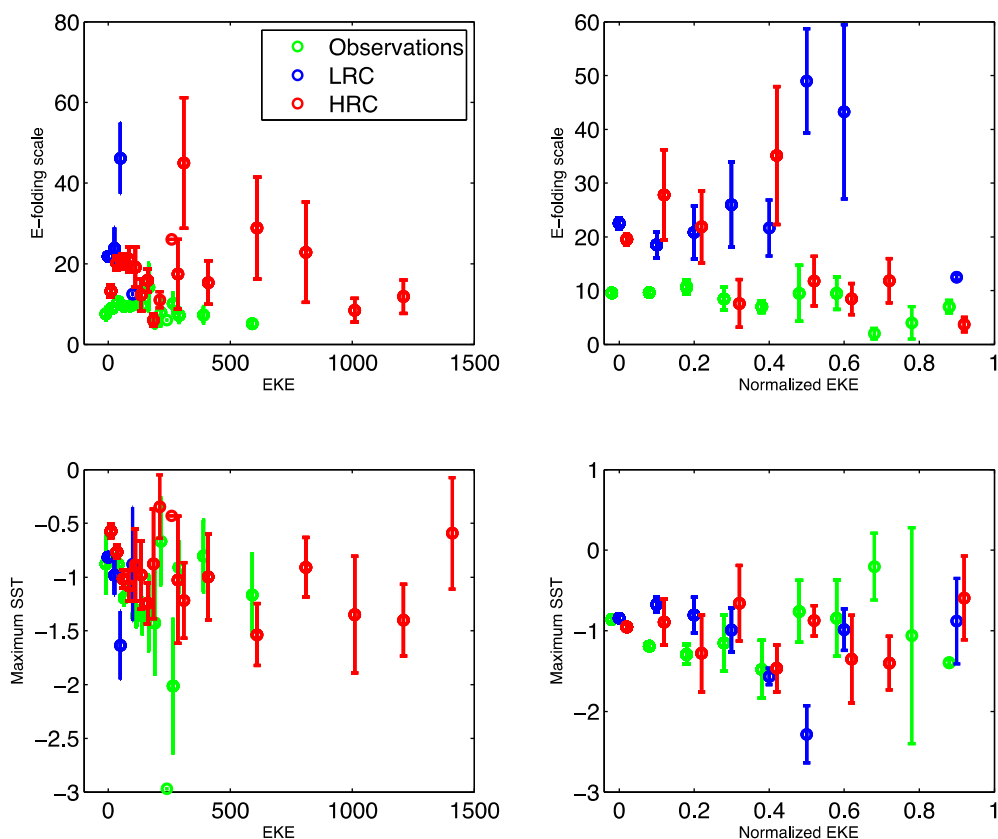


Figure 9. Relationship (top) between EKE and e -folding time and (bottom) between EKE and maximum sea surface cooling in observations (green), low-resolution simulation (blue), and high-resolution simulation (red). The circles are bin averages and the error bars are their respective standard errors. EKE is normalized on the right figures.

$PW = 10^{15}$ W) and 0.06 ± 0.005 PW, respectively. In order to make a comparison between the model and observations, we compare the model results with 60% of the total basin-scale OHC in the observations, since the TC number in the model is about 60% of the observational record in the Northwestern Pacific basin (see Table 1). Due to the lack of observational estimates of latent heat fluxes within TCs, we apply $F = 0.55$ from the model for the observational OHC calculation. The annual surface flux-corrected basin-scale OHC for all the storm intensities in the observations is 0.35×10^{22} J, and 60% of which is 0.21×10^{22} J. This value is comparable with the modeled results. These first-order estimates suggest that the coupled model is capable of capturing realistic surface heat fluxes and the upper-ocean heat convergence responses to tropical cyclones. These preliminary results point to the potential importance of using high-resolution coupled modeling approaches to advance our understanding about tropical cyclones and climate.

4. Caveats

This study includes several important simplifying assumptions and caveats, in addition to the methodological constraints discussed in section 2. Although the 0.5° resolution atmosphere model is shown to be capable of capturing realistic TC circulations and spatial distributions in the Northwestern Pacific, the storm intensities are likely to be underestimated. Thus, potential differences in the storm-induced responses for extremes storms cannot be examined using this model.

Shear instability induced by near-inertial waves contributes to TC-induced SST cooling through turbulent entrainment at the base of the mixed layer [Cuyper *et al.*, 2013; Ginis, 2002]. This effect is dependent on the magnitude of near-inertial energy input by the winds to the ocean, as well as the dissipation of the near-inertial energy beneath the oceanic boundary layer. The modeled near-inertial energy input by the winds is highly dependent on the resolution of the atmospheric component and on the coupling frequency [Jiang *et al.*, 2005; Jochum *et al.*, 2013]. The atmospheric model considered here (0.5°) is not capable of simulating

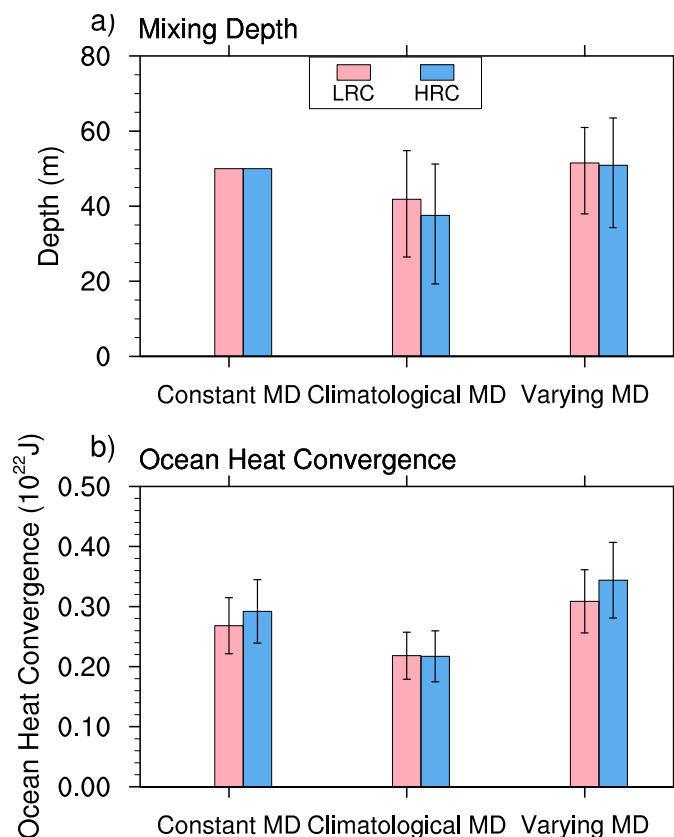


Figure 10. (a) Composite area-mean mixing depth of each storm day in the Northwest Pacific basin for low-resolution simulation (LRC) and high-resolution simulation (HRC), computed with three strategies: (left to right) constant mixing depth of 50 m, monthly mean climatological mixed-layer depth, and varying mixing depth derived from ocean potential temperature profiles. The averaging area is a 6° × 6° grid box. The error bars indicate the range of mixing depth within the averaging area for the analysis period (20 years). (b) Annually accumulated, storm-induced average ocean heat uptake in the Northwest Pacific basin, computed with the three corresponding mixing depth strategies. A discrete method is used to account for the nonuniform mixing within the 6° × 6° averaging domain. Error bars represent the plus or minus 1 standard deviation.

extreme TC events or the fine-scale atmospheric frontal features that can be important for generating near-inertial energy input to the ocean. Under this situation, the KPP vertical mixing parameterization scheme used in the model would not provide sufficient near-inertial wave-induced shears [Large et al., 1994; Jochum et al., 2013]. A parameterization for the dissipation of near-inertial energy in the upper ocean is not applied in the present (CCSM3.5) or in more recent versions of this model [Jochum et al., 2013]. Improved representation of this effect could impact mixed-layer depth, SST, and precipitation patterns [Jochum et al., 2013]. Whether the results presented here would change under improved representation of near-inertial waves in the model is an open question, which will be the topic of a future paper.

The effect of mesoscale eddies on ocean surface cooling due to entrainment would also likely depend on the vertical resolution. Both simulations feature the same relatively coarse vertical resolution (42 levels). Increasing vertical resolution (particularly near the surface) may induce a stronger eddy effect on surface cooling that is not captured here.

5. Conclusions

Upper-ocean responses to TCs in a fully coupled Earth system model with varying horizontal ocean grid resolution are investigated in this paper. We analyzed the resolution-dependent responses by examining simulated TC climatologies, sea surface cooling responses, and latent heat budgets. We estimate TC-induced OHC in the Northwestern Pacific for both model configurations from near-surface atmosphere and

ocean fields using multiple strategies accounting for uncertainties in vertical mixing length scales.

Results indicate that the ocean surface responses and basin-scale aggregated TC influences on upper-ocean heat budgets within the coupled model configurations considered here are relatively insensitive to the choice of ocean grid resolution, when considering

Data	LRC	HRC
Latent heat exchange (J)	1.43e + 21	1.70e + 21
Total OHC (J)	3.08e + 21	3.57e + 21
Percentage of latent heat flux in total OHC	45%	47%
Mixing-induced OHC (J)	1.65e + 21	1.87e + 21
Mixing-induced OHC (PW)	0.05	0.06
Standard deviation of the distribution of annual OHC	0.02143	0.03351

1° versus 0.1° resolution. This suggests that the surface eddy flux parameterization in the low-resolution model may be sufficient for capturing the basin-scale horizontal temperature distribution and heat transport induced by mesoscale eddies [Danabasoglu *et al.*, 2008]. However, it is important to consider limitations in the ocean model's representation of near-inertial wave response when interpreting these results, as well as relatively coarse (0.5°) atmosphere model resolution which is unable to simulate frontal systems important for near-inertial energy input to the ocean. TC-induced ocean sensitivities to horizontal grid resolution may emerge with improved representation of near-inertial waves, which could influence transient intraseasonal dynamic responses to TC forcing as well as poststorm wake recovery, ocean heat uptake, upper-ocean currents, and meridional transports.

Given the magnitude of the modeled and observed TC-induced fluxes of heat and momentum at the atmosphere-ocean interface, and the resulting positive ocean heat convergence, these results point to the importance of coupled model approaches to developing a more complete understanding about the relationship between TCs and climate. Coupled modeling initiatives utilizing ultra-high-resolution modeling frameworks may provide fundamental insight to potential TC-induced feedbacks that influence large-scale ocean and atmosphere heat budgets and circulation patterns.

Acknowledgments

We thank Ben Kirtman for providing the model output for the analyses in this study. Marlos Goes was partly supported by NOAA/AOML and the NOAA Climate Program Office. We also thank Kerry Emanuel for providing global TC best track data: <http://eaps4.mit.edu/faculty/Emanuel/products>. The OI SST product is from the Remote Sensing System website (<http://www.remss.com/>) and is sponsored by National Oceanographic Partnership Program (NOPP), the NASA Earth Science Physical Oceanography Program, and the NASA MEaSUREs DISCOVER Project. The ORAS4 ocean reanalysis data are provided by the Asia-Pacific Data-Research Center of the International Pacific Research Center, which can be found on their website at <http://apdrc.soest.hawaii.edu/data/data.php>. The WOA13 product is provided by NOAA National Oceanographic Data Center. The wind shear climatology is from NCEP Reanalysis, which is provided by the NOAA/OAR/ESRL PSD, Boulder, Colorado, USA, from their website at <http://www.esrl.noaa.gov/psd/>. The altimeter products were produced by Ssalto/Duacs and distributed by Aviso with support from Cnes.

References

- Bacmeister, J. T., M. F. Wehner, R. B. Neale, A. Gettelman, C. Hannay, P. H. Lauritzen, J. M. Caron, and J. E. Truesdale (2013), Exploratory high-resolution climate simulations using the community atmosphere model (CAM), *J. Clim.*, *27*(9), 3073–3099, doi:10.1175/JCLI-D-13-00387.1.
- Bell, R., J. Strachan, P. L. Vidale, K. Hodges, and M. Roberts (2013), Response of tropical cyclones to idealized climate change experiments in a global high-resolution coupled general circulation model, *J. Clim.*, *26*(20), 7966–7980, doi:10.1175/JCLI-D-12-00749.1.
- Bender, M. A., and I. Ginis (2000), Real-case simulations of hurricane-ocean interaction using a high-resolution coupled model: Effects on hurricane intensity, *Mon. Weather Rev.*, *128*(4), 917–946.
- Boos, W. R., J. R. Scott, and K. A. Emanuel (2004), Transient diapycnal mixing and the meridional overturning circulation, *J. Phys. Oceanogr.*, *34*(1), 334–341, doi:10.1175/1520-0485(2004)034<0334:TDMATM>2.0.CO;2.
- Bueti, M. R., I. Ginis, L. M. Rothstein, and S. M. Griffies (2014), Tropical cyclone-induced thermocline warming and its regional and global impacts, *J. Clim.*, *27*, 6978–6999, doi:10.1175/JCLI-D-14-00152.1.
- Camargo, S. J. (2013), Global and regional aspects of tropical cyclone activity in the CMIP5 models, *J. Clim.*, *26*(24), 9880–9902, doi:10.1175/JCLI-D-12-00549.1.
- Camargo, S. J., and S. E. Zebiak (2002), Improving the detection and tracking of tropical cyclones in atmospheric general circulation models, *Weather Forecasting*, *17*(6), 1152–1162.
- Camargo, S. J., A. G. Barnston, and S. E. Zebiak (2005), A statistical assessment of tropical cyclone activity in atmospheric general circulation models, *Tellus, Ser. A*, *57*(4), 589–604, doi:10.3402/tellusa.v57i4.14705.
- Chelton, D. B., R. A. deSzoeke, M. G. Schlax, K. E. I. Naggar, N. Siwertz (1998), Geographical variability of the first baroclinic Rossby radius of deformation, *J. Phys. Oceanogr.*, *28*, 433–460.
- Cheng, L., J. Zhu, and R. L. Striver (2014), Global representation of tropical cyclone-induced ocean thermal changes using Argo data—Part 1: Methods and results, *Ocean Sci. Discuss.*, *11*(6), 2831–2878, doi:10.5194/osd-11-2831-2014.
- Cuyppers, Y., X. Le Vaillant, P. Bouruet-Aubertot, J. Vialard, and M. J. McPhaden (2013), Tropical storm-induced near-inertial internal waves during the Cirene experiment: Energy fluxes and impact on vertical mixing, *J. Geophys. Res. Oceans*, *118*, 358–380, doi:10.1029/2012JC007881.
- Danabasoglu, G., R. Ferrari, and J. C. McWilliams (2008), Sensitivity of an Ocean General Circulation Model to a Parameterization of Near-Surface Eddy Fluxes, *J. Clim.*, *21*(6), 1192–1208, doi:10.1175/2007JCLI1508.1.
- Danabasoglu, G., S. C. Bates, B. P. Briegleb, S. R. Jayne, M. Jochum, W. G. Large, S. Peacock, and S. G. Yeager (2012), The CCSM4 ocean component, *J. Clim.*, *25*(5), 1361–1389, doi:10.1175/JCLI-D-11-00091.1.
- Dare, R. A., and J. L. McBride (2011), Sea surface temperature response to tropical cyclones, *Mon. Weather Rev.*, *139*(12), 3798–3808, doi:10.1175/MWR-D-10-05019.1.
- D'Asaro, E. A., T. B. Sanford, P. P. Niiler, and E. J. Terrill (2007), Cold wake of Hurricane Frances, *Geophys. Res. Lett.*, *34*, L15609, doi:10.1029/2007GL030160.
- Emanuel, K. (2001), Contribution of tropical cyclones to meridional heat transport by the oceans, *J. Geophys. Res.*, *106*(D14), 14,771–14,781, doi:10.1029/2000JD900641.
- Gent, P. R., S. G. Yeager, R. B. Neale, S. Levis, and D. A. Bailey (2010), Improvements in a half degree atmosphere/land version of the CCSM, *Clim. Dyn.*, *34*(6), 819–833, doi:10.1007/s00382-009-0614-8.
- Gentemann, C. L., T. Meissner, and F. J. Wentz (2010), Accuracy of satellite sea surface temperatures at 7 and 11 GHz, *IEEE Trans. Geosci. Remote Sens.*, *48*(3), 1009–1018, doi:10.1109/TGRS.2009.2030322.
- Ginis, I. (2002), Tropical cyclone-ocean interactions, *Adv. Fluid Mech.*, *33*, 83–114.
- Gualdi, S., E. Scoccimarro, and A. Navarra (2008), Changes in tropical cyclone activity due to global warming: Results from a high-resolution coupled general circulation model, *J. Clim.*, *21*(20), 5204–5228, doi:10.1175/2008JCLI1921.1.
- Haney, S., S. Bachman, B. Cooper, S. Kupper, K. McCaffrey, L. Van Roekel, S. Stevenson, B. Fox-Kemper, and R. Ferrari (2012), Hurricane wake restratification rates of one-, two- and three-dimensional processes, *J. Mar. Res.*, *70*(6), 824–850.
- Hart, R. E. (2011), An inverse relationship between aggregate northern hemisphere tropical cyclone activity and subsequent winter climate, *Geophys. Res. Lett.*, *38*, L01705, doi:10.1029/2010GL045612.
- Hu, A., and G. A. Meehl (2009), Effect of the Atlantic hurricanes on the oceanic meridional overturning circulation and heat transport, *Geophys. Res. Lett.*, *36*, L03702, doi:10.1029/2008GL036680.
- Huang, P., T. B. Sanford, and J. Imberger (2009), Heat and turbulent kinetic energy budgets for surface layer cooling induced by the passage of Hurricane Frances (2004), *J. Geophys. Res.*, *114*, C12023, doi:10.1029/2009JC005603.

- Jansen, M., and R. Ferrari (2009), Impact of the latitudinal distribution of tropical cyclones on ocean heat transport, *Geophys. Res. Lett.*, *36*, L06604, doi:10.1029/2008GL036796.
- Jansen, M. F., R. Ferrari, and T. A. Mooring (2010), Seasonal versus permanent thermocline warming by tropical cyclones, *Geophys. Res. Lett.*, *37*, L03602, doi:10.1029/2009GL041808.
- Jiang, J., Y. Liu, and W. Perrie (2005), Estimating the energy flux from the wind to ocean inertial motions: The sensitivity to surface wind fields, *Geophys. Res. Lett.*, *32*, L15610–2844, doi:10.1029/2005GL023289.
- Jochum, M., B. P. Briegleb, G. Danabasoglu, W. G. Large, N. J. Norton, S. R. Jayne, M. H. Alford, and F. O. Bryan (2013), The Impact of Oceanic Near-Inertial Waves on Climate, *J. Clim.*, *26*(9), 2883–2844, doi:10.1175/JCLI-D-12-00181.1.
- Jullien, S., C. E. Menkes, P. Marchesiello, N. C. Jourdain, M. Lengaigne, A. Koch-Larrouy, J. Lefèvre, E. M. Vincent, and V. Faure (2012), Impact of tropical cyclones on the heat budget of the South Pacific Ocean, *J. Phys. Oceanogr.*, *42*(11), 1882–1906, doi:10.1175/JPO-D-11-0133.1.
- Jullien, S., P. Marchesiello, C. E. Menkes, J. Lefèvre, N. C. Jourdain, G. Samson, and M. Lengaigne (2014), Ocean feedback to tropical cyclones: Climatology and processes, *Clim. Dyn.*, *43*, 2831–2854, doi:10.1007/s00382-014-2096-6.
- Killworth, P. D. (1997), On the parameterization of eddy transfer, part I: Theory, *J. Mar. Res.*, *55*, 1171–1197, doi:10.1357/0022240973224102.
- Kim, H.-S., G. A. Vecchi, T. R. Knutson, W. G. Anderson, T. L. Delworth, A. Rosati, F. Zeng, and M. Zhao (2014), Tropical cyclone simulation and response to CO₂ doubling in the GFDL CM2.5 high-resolution coupled climate model, *J. Clim.*, *27*, 8034–8054, doi:10.1175/JCLI-D-13-00475.1.
- Kirtman, B. P., et al. (2012), Impact of ocean model resolution on CCSM climate simulations, *Clim. Dyn.*, *39*(6), 1303–1328, doi:10.1007/s00382-012-1500-3.
- Large, W. G., J. C. McWilliams, and S. C. Doney (1994), Oceanic vertical mixing: A review and a model with a nonlocal boundary layer parameterization, *Rev. Geophys.*, *32*, 363–403.
- Locarnini, R. A., et al. (2013), World Ocean Atlas 2013, Volume 1: Temperature, S. Levitus, Ed., A. Mishonov Technical Ed., NOAA Atlas NESDIS 73, 40 pp.
- Le Traon, P. Y., F. Nadal, and N. Ducet (1998), An improved mapping method of multisatellite altimeter data, *J. Atmos. Oceanic Technol.*, *15*(2), 522–534.
- Li, F., W. D. Collins, M. F. Wehner, and L. R. Leung (2013), Hurricanes in an aquaplanet world: Implications of the impacts of external forcing and model horizontal resolution, *J. Adv. Model. Earth Syst.*, *5*, 134–145, doi:10.1002/jame.20020.
- Liu, J., J. A. Curry, C. A. Clayson, and M. A. Bourassa (2011), High-resolution satellite surface latent heat fluxes in North Atlantic Hurricanes, *Mon. Weather Rev.*, *139*(9), 2735–2747, doi:10.1175/2011MWR3548.1.
- Lloyd, I. D., and G. A. Vecchi (2011), Observational evidence for oceanic controls on hurricane intensity, *J. Clim.*, *24*(4), 1138–1153, doi:10.1175/2010JCLI3763.1.
- Maltrud, M. E., and J. L. McClean (2005), An eddy resolving global 1/10° ocean simulation, *Ocean Modell.*, *8*(1–2), 31–54, doi:10.1016/j.ocemod.2003.12.001.
- Manganello, J. V., et al. (2012), Tropical cyclone climatology in a 10-km global atmospheric GCM: Toward weather-resolving climate modeling, *J. Clim.*, *25*(11), 3867–3893, doi:10.1175/JCLI-D-11-00346.1.
- Manucharyan, G. E., C. M. Brierley, and A. V. Fedorov (2011), Climate impacts of intermittent upper ocean mixing induced by tropical cyclones, *J. Geophys. Res. Oceans*, *116*(C11), C11038–30, doi:10.1029/2011JC007295.
- McClean, J. L., et al. (2011), A prototype two-decade fully-coupled fine-resolution CCSM simulation, *Ocean Modell.*, *39*(1–2), 10–30, doi:10.1016/j.ocemod.2011.02.011.
- Mei, W., and C. Pasquero (2012), Spatial and temporal characterization of sea surface temperature response to tropical cyclones, *J. Clim.*, *26*(11), 3745–3765, doi:10.1175/JCLI-D-12-00125.1.
- Mei, W., F. Primeau, J. C. McWilliams, and C. Pasquero (2013), Sea surface height evidence for long-term warming effects of tropical cyclones on the ocean, *Proc. Natl. Acad. Sci. U. S. A.*, *110*, 15,207–15,210, doi:10.1073/pnas.1306753110.
- Murakami, H., and M. Sugi (2010), Effect of model resolution on tropical cyclone climate projections, *SOLA*, *6*, 73–76, doi:10.2151/sola.2010-019.
- Park, J. J., Y.-O. Kwon, and J. F. Price (2011), Argo array observation of ocean heat content changes induced by tropical cyclones in the north Pacific, *J. Geophys. Res.*, *116*, C12025, doi:10.1029/2011JC007165.
- Pasquero, C., and K. Emanuel (2008), Tropical cyclones and transient upper-ocean warming, *J. Clim.*, *21*(1), 149–162, doi:10.1175/2007JCLI1550.1.
- Rathmann, N. M., S. Yang, and E. Kaas (2014), Tropical cyclones in enhanced resolution CMIP5 experiments, *Clim. Dyn.*, *42*(3–4), 665–681, doi:10.1007/s00382-013-1818-5.
- Scoccimarro, E., S. Gualdi, A. Bellucci, A. Sanna, P. Giuseppe Fogli, E. Manzini, M. Vichi, P. Oddo, and A. Navarra (2011), Effects of tropical cyclones on ocean heat transport in a high-resolution coupled general circulation model, *J. Clim.*, *24*(16), 4368–4384, doi:10.1175/2011JCLI4104.1.
- Shaevitz, D. A., et al. (2014), Characteristics of tropical cyclones in high-resolution models in the present climate, *J. Adv. Model. Earth Syst.*, *6*, 1154–1172, doi:10.1002/2014MS000372.
- Small, R. J., et al. (2014), A new synoptic scale resolving global climate simulation using the Community Earth System Model, *J. Adv. Model. Earth Syst.*, *6*, 1065–1094, doi:10.1002/2014MS000363.
- Smith, R. D., M. E. Maltrud, F. O. Bryan, and M. W. Hecht (2000), Numerical simulation of the North Atlantic Ocean at 1/10°, *J. Phys. Oceanogr.*, *30*(7), 1532–1561, doi:10.1175/1520-0485(2000)030<1532:NSOTNA>2.0.CO;2.
- Striver, R. L. (2013), Observational evidence supports the role of tropical cyclones in regulating climate, *Proc. Natl. Acad. Sci. U. S. A.*, *110*(38), 15,173–15,174, doi:10.1073/pnas.1314721110.
- Striver, R. L., and M. Huber (2007), Observational evidence for an ocean heat pump induced by tropical cyclones, *Nature*, *447*(7144), 577–580, doi:10.1038/nature05785.
- Striver, R. L., and M. Huber (2010), Modeled sensitivity of upper thermocline properties to tropical cyclone winds and possible feedbacks on the Hadley circulation, *Geophys. Res. Lett.*, *37*, L08704, doi:10.1029/2010GL02836.
- Striver, R. L., M. Huber, and J. Nusbaumer (2008), Investigating tropical cyclone-climate feedbacks using the TRMM Microwave Imager and the Quick Scatterometer, *Geochem. Geophys. Geosyst.*, *9*, Q09V11, doi:10.1029/2007GC001842.
- Striver, R. L., M. Goes, M. E. Mann, and K. Keller (2010), Climate response to tropical cyclone-induced ocean mixing in an Earth system model of intermediate complexity, *J. Geophys. Res.*, *115*, C10042, doi:10.1029/2010JC006106.
- Strachan, J., P. L. Vidale, K. Hodges, M. Roberts, and M.-E. Demory (2012), Investigating global tropical cyclone activity with a Hierarchy of AGCMs: The role of model resolution, *J. Clim.*, *26*(1), 133–152, doi:10.1175/JCLI-D-12-00012.1.
- Vincent, E. M., M. Lengaigne, J. Vialard, G. Madec, N. C. Jourdain, and S. Masson (2012a), Assessing the oceanic control on the amplitude of sea surface cooling induced by tropical cyclones, *J. Geophys. Res.*, *117*(C5), doi:10.1029/2011JC007705.

- Vincent, E. M., M. Lengaigne, G. Madec, J. Vialard, G. Samson, N. C. Jourdain, C. E. Menkes, and S. Jullien (2012b), Processes setting the characteristics of sea surface cooling induced by tropical cyclones, *J. Geophys. Res.*, *117*(C2), doi:10.1029/2011JC007396.
- Vincent, E. M., G. Madec, M. Lengaigne, J. Vialard, and A. Koch-Larrouy (2013), Influence of tropical cyclones on sea surface temperature seasonal cycle and ocean heat transport, *Clim. Dyn.*, *41*(7–8), 2019–2038, doi:10.1007/s00382-012-1556-0.
- Walsh, K., S. Lavender, E. Scoccimarro, and H. Murakami (2013), Resolution dependence of tropical cyclone formation in CMIP3 and finer resolution models, *Clim. Dyn.*, *40*(3–4), 585–599, doi:10.1007/s00382-012-1298-z.
- Wang, X., C. Wang, G. Han, W. Li, and X. Wu (2014), Effects of tropical cyclones on large-scale circulation and ocean heat transport in the South China Sea, *Clim. Dyn.*, *43*, 3351–3366, doi:10.1007/s00382-014-2109-5.
- Wehner, M. F., G. Bala, P. Duffy, A. A. Mirin, and R. Romano (2010), Towards direct simulation of future tropical cyclone statistics in a high-resolution global atmospheric model, *Adv. Meteorol.*, *2010*, 915303, doi:10.1155/2010/915303.
- Wehner, M. F., et al. (2014), The effect of horizontal resolution on simulation quality in the community atmospheric model, CAM5.1, *J. Adv. Model. Earth Syst.*, *6*, 980–997, doi:10.1002/2013MS000276.
- Zhao, M., I. M. Held, S.-J. Lin, and G. A. Vecchi (2009), Simulations of global hurricane climatology, interannual variability, and response to global warming using a 50-km resolution GCM, *J. Clim.*, *22*(24), 6653–6678, doi:10.1175/2009JCLI3049.1.